Journal of the European Ceramic Society 43 (2023) 5413–5424

Contents lists available at ScienceDirect

Journal of the European Ceramic Society

journal homepage: www.elsevier.com/locate/jeurceramsoc

Tribological behavior of carbon fiber reinforced ZrB_2 based ultra high temperature ceramics

Matteo Mor [a,*,1], Matthias Meiser [b,*,1], Nico Langhof [b], Antonio Vinci [a], Simone Failla [a], Bettina Alber-Laukant [c], Stephan Tremmel [c], Stefan Schafföner [b], Diletta Sciti [a]

[a] CNR-ISTEC, Institute of Science and Technology for Ceramics, 48018 Faenza, Italy
[b] Chair of Ceramic Materials Engineering, University of Bayreuth, 95447 Bayreuth, Germany
[c] Engineering Design and CAD, University of Bayreuth, 95447 Bayreuth, Germany

ARTICLE INFO

Keywords:
UHTCMC
ZrB_2
Tribological properties
Carbon fiber

ABSTRACT

The tribological behavior of ultra-high temperature ceramic matrix composites (UHTCMCs) was investigated to understand these materials in friction applications. Samples consisting of pitch-based randomly orientated chopped carbon fiber (CF) reinforced ZrB_2-10 vol% SiC were prepared (ZS). The tribological behavior was tested on a self-designed dynamometer, coupling the UHTCMC pads with either carbon fiber reinforced carbon–silicon carbide (C/C-SiC) or steel disks, with two applied contact pressures (1 and 3 MPa) and the surface microstructures were analyzed to unravel the wear mechanisms. Even at high mechanical stresses, tests against the C/C-SiC disk showed stable braking performance and wear. The abraded material from a steel disk formed a stable friction film by fusing together harder pad particles with abraded steel, which reduced wear and stabilized the braking performance. The high values of coefficient of friction obtained (0.5–0.7), their stability during the braking and the acceptable wear rate make these materials appealing for automotive brake applications.

1. Introduction

Ultra-high temperature ceramic matrix composites (UHTCMCs) are a class of refractory ceramics capable of operating in extreme environments (e.g. temperature above 2000 °C, high heat fluxes, > 10 MW/m^2) [1]. They consist of borides, carbides and nitrides of early transition metals, which are characterized by a melting point above 3000 °C [2]. Amongst ultra-high temperature ceramics (UHTCs), ZrB_2 is the most interesting compound because it combines a relatively low density with high melting point, high strength and good electrical conductivity [3,4]. However, the oxidation resistance of pure ZrB_2 is poor due to the formation of ZrO_2 and evaporation of B_2O_3 above 1000 °C [5]. To overcome this problem, previous studies investigated additives such as silicon carbide (SiC) or other silicides that protect the material from oxidation up to 1600 °C due to the formation of a glassy silica phase [6,7]. Another main problem of ZrB_2 based ceramics is their low fracture toughness [8], which limits their applicability when thermal shock and vibrations are present [9]. An effective method to improve their damage tolerance has become the addition of short and long fibers, such as carbon fibers (CF) [10–14]. On the other hand, the fiber reinforcement also lowers the strength of the composite [15,16]. Thanks to their high melting point, high oxidation resistance, good room and high temperature strength, carbon fiber reinforced UHTC materials are of great interest in the field of aerospace applications, in extreme environments associated with hypersonic flight, atmospheric re-entry, rocket propulsion, plasma arc electrodes and heating elements [17–19].

With these promising properties, these materials can be also considered for other applications including as friction materials. To date, UHTCs were analyzed in a number of papers regarding their wear behavior in different pin-on-disk configurations [20–28]. Some of the authors of the present work have recently investigated the wear and friction behavior of monolithic ZrB_2 pin on ZrB_2-SiC disk, reporting a high friction coefficient that could be exploited for brake applications [29].

A lot of research is currently being conducted in the field of braking systems because of the advance of electric cars with different operating conditions [30]. With performance brake materials for the use in vehicles, the main requirements are high and stable coefficients of friction

* Corresponding authors.
E-mail addresses: matteo.mor@issmc.cnr.it (M. Mor), matthias.meiser@uni-bayreuth.de (M. Meiser).
[1] These authors contributed equally to this work.

https://doi.org/10.1016/j.jeurceramsoc.2023.05.019
Received 22 March 2023; Received in revised form 10 May 2023; Accepted 11 May 2023
Available online 12 May 2023

(COF) under multiple braking conditions, low wear rate for increased life, low life cycle cost, low weight, good noise, vibration and harshness properties (NVH) and a high degree of freedom in the structural design [31,32]. For vehicles, brakes are generally used in a pad on disk configuration. Common disk materials include steel and gray cast iron, carbon-carbon (C/C) and carbon fiber reinforced carbon-silicon carbide (C/C-SiC). Steel and gray cast iron are used for standard automotive and train braking systems. These materials are cheap, possess a relatively high and stable coefficient of friction and low wear rate [33]. Paired with organic or metallic pads they suit all but high-performance applications, where a low operating temperature (≈ 400 °C [34]) and high metal density would cause big brakes with high unsprung masses. Therefore, C/Cs were developed in the 1970 s and have been used ever since in aircrafts and racing vehicles e.g., Formula 1 and Formula E.

A density of less than 2 g/cm^3 , high maximum operating temperatures (2000 °C) combined with high heat capacity and thermal shock resistance make light brakes capable of absorbing huge amounts of energy in a short time [35]. However, C/C materials start to oxidize significantly at 600 °C and possess low COF in wet or cold conditions due to the inherent lubrication ability of graphite [35,36]. These disadvantages make them unsuitable for standard road vehicles. To overcome these problems, C/C-SiC composites, developed since the 1990 s, are manufactured by liquid silicon infiltration (LSI) of C/C and used in high performance cars [37]. These CMCs exhibit exceptional wear resistance, less oxidation and a high COF in different weather conditions at the expense of weight and limited operating temperature [36]. C/C-SiC disks are usually paired with organic or metallic pads with some research being carried out on ceramic pads for full-ceramic brake systems [38,39], but with C/C-SiC pads still having hard vibration harshness (NVH) and high thermal conductivity issues.

The presence of SiC can increase the coefficient of friction, the thermal shock resistance and the environmental stability [40]. However, at the same time, the presence of SiC may increase the wear rate due to abrasion and may also decrease the fatigue resistance depending on the pad material [41,42]. Moreover, C/C-SiC brake disks paired with common pad materials may suffer from instability of the coefficient of friction during braking [31], which is often noted as saddle-curve behavior resulting in rising COF for low and high sliding speeds during a braking cycle [31]. The introduction of different ceramic phases could ensure broader adjustment of tribological properties. Moreover, hybrid ceramics can increase the friction resistance. For example, in a ZrB_2 carbon fiber reinforced material, the carbon fibers play the role of a lubricant to prevent clogging during braking, whereas the ZrB_2 can rapidly form an oxide layer during braking to prevent carbon fiber oxidation. Their joint effects was attributed to a braking performance with higher stability [43]. For these reasons carbon fiber reinforced ZrB_2-based materials could be a new class of materials for braking applications.

Based on the above analysis, this paper investigated the tribological behavior of carbon fiber reinforced, UHTC-ZrB_2 based materials on steel and C/C-SiC disks. The COF, wear and temperatures were recorded at different braking pressures of 1 and 3 MPa. SEM, EDX and XRD analysis were carried out in order to determine the friction layer formation and to explain corresponding tribological results.

2. Materials and methods

2.1. Preparation of braking samples

All UHTCMC sample materials consisted of a matrix of ZrB_2 (H.C. Starck, grade B, Germany, specific surface area 1.0 m^2/g, particle size range 0.5–6 μm, impurities (wt%): 0.25 C, 2 O, 0.25 N, 0.1 Fe, 0.2 Hf, ρ = 6.10 g/cm^3) and α-SiC (H.C. Starck, Grade UF-25, Germany, specific surface area 23 – 26 m^2/g, D50 = 0.45 μm; Italian retailer: Metalchimica, ρ = 3.21 g/cm^3). As a reinforcement, pitch based high modulus (HM) carbon fibers (Granoc Yarn XN80–6 K fibers; tensile modulus of 780 GPa and tensile strength 3.4 GPa, 10 μm diameter, ρ = 2.17 g/cm^3) were used.

The pads (ZS) were made of ZrB_2-10 vol% SiC ceramics reinforced with 35 vol% randomly oriented chopped pitch carbon fibers with a median length of 5 mm. The samples were produced by slurry infiltration of chopped fibers (Fig. 1). The layers with random XY-plane fiber orientation were piled up and hot pressed at 1900 °C using a pressure of 35 MPa, in accordance with previous investigations [44].

The sample compositions are summarized in Table 1. To obtain the final sample dimensions, the material was cut, and the surface was ground (Ra= 0.609 μm ± 0.166 μm; Rt= 3.55 μm ± 1.00 μm). In the end, 10 mm thick pads with a surface area of 900 mm^2 (30 mm × 30 mm) were obtained, see Fig. 2.

2.2. Experimental procedures

Before the friction analysis, the bulk density and open porosity were measured. The bulk density was measured by Archimedes method according to DIN EN 1389:2003 in distilled water. The mercury intrusion porosimetry (MIP) analysis was carried out to determine the amount of open porosity (Pascal 140 and Pascal 240 series, Thermo Finnigan, USA). The 4-point flexural strength and the chevron-notched beam fracture toughness of the pad material were investigated in previous studies relative to the processing of these materials [44]. The four-point bending strength tests were carried out on test bars 25 × 2.5 × 2 mm^3 (length by width by thickness, respectively) according to the standard ISO/DIS 14704. The fracture toughness (K_{Ic}) was determined by four-point chevron notch bending tests (CNB). Thus, the test bars of 25 × 2 × 2.5 mm^3 (length by width by thickness, respectively) were notched with a 0.1 mm-thick diamond saw. For each material, at least three bars were tested.

Tribological tests were conducted on a self-designed inertia dynamometer, which is illustrated in Fig. 3. For one cycle, the flywheel with a mass of 800 kg (inertia moment of 96 kgm^2) was accelerated by a 45 kW motor in about 20 s to 1030 rpm and then the motor was switched off. Then the pneumatic brake caliper was applied with a surface pressure of 1 or 3 MPa to a complete stop. The next cycle was then started immediately. Braking energy per 10 braking cycles summed up to 5.43 MJ with different sliding speeds due to the different friction radius of tested C/C-SiC and steel disks.

With each test, two braking pads (30 × 30 × 10 mm^3) were tested against commercial and self-made (machined) disks as counterparts:

- Commercial, internally ventilated C/C-SiC brake disk with SiC-rich friction layer (SGL, Germany), friction radius of 184 mm; diameter 400 mm; thickness 39 mm. This design represents the state-of-the-art in C/C-SiC-based braking technology.
- Self-made, solid steel brake disk, constituted by S235 Steel, friction radius of 173 mm; diameter 380 mm; thickness 40 mm. The common S235 unalloyed Steel, non-ventilated disk was used as a base for different iron-based brake disk materials.

Each braking test consisted of 10 braking cycles to a complete stop. Before each test, 5 pre-braking cycles were conducted. The system was then cooled down to ≤ 30 °C. The mass and thickness of the braking pads were measured at four points before and after each braking test to calculate the volumetric and mass specific wear rates. The temperatures were recorded continuously on the backside of both pads as well as on both sliding surfaces on the disk by type-K sliding thermocouples. The COF was calculated by continually measuring the clamp pressure and braking torque with 100 Hz. The conditions during braking are summarized in Table 2.

2.3. Microstructure analysis

The microstructure was analyzed before and after the friction tests. Before the tests, the microstructures were studied on the polished

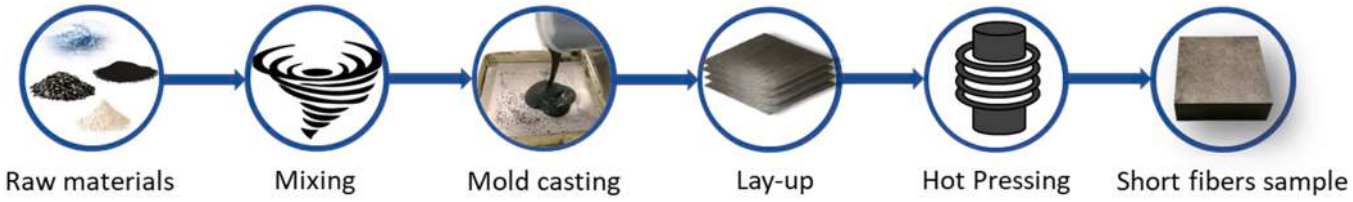

Fig. 1. Flow chart of the processes used to obtain the samples chopped fiber reinforcement.

Table 1
Matrix composition of the samples, content and length of carbon fibers and their orientation.

Sample (unit)	ZrB_2 (vol%)	SiC (vol%)	Fiber amount (vol%)	Fiber length (mm)	Fiber distribution
ZS	90	10	35 ± 5	5	random

surface by a field emission scanning electron microscope (FE-SEM, Carl Zeiss Sigma NTS GmbH, Oberkochen, Germany) at CNR-ISSMC (formerly ISTEC) of Faenza (Italy). The samples were observed in the XY and XZ-surface in order to analyze the microstructure of the different fiber orientations.

After the friction tests, the microstructure and composition were observed without further treatment on the XY-surface to investigate the friction layer. The analysis was conducted at the University of Bayreuth (Germany) and at CNR-ISSMC (Italy) with a SEM (Gemini Sigma 300 VP, Zeiss, Germany and FE-SEM, Zeiss, Germany) and energy dispersive X-ray spectroscopy (EDX, Octane Super, EDAX Ametek, USA and EDX, INCA Energy 300, Oxford instruments, UK). X-ray diffraction analysis was carried out on the materials before and after the tests (Bruker D8 Advance apparatus, Karlsruhe, Germany) collecting patterns from 10° to 80° (step 0.02°, step time 0.5 s), with a measurement area of 14 × 16 mm and a depth of 1–5 μm.

3. Results and discussion

3.1. Microstructural features and mechanical properties

A summary of the bulk densities, open porosities and the mechanical properties, flexural strength and fracture toughness, are reported in Table 3.

The microstructures of the surface and cross section before the tribological tests are shown in Fig. 4. The light gray and dark gray phases represent ZrB_2 and SiC respectively, while the carbon fibers are black. The matrix was nearly fully dense, with few pores around the fibers (Fig. 4b). The surface (XY plane) shows the random fiber distribution resulting from the novel slurry-based process (Fig. 1). From the cross section of the sample (Fig. 4a) it is possible to notice the anisotropy consistently with the process adopted. The fibers were still homogeneously dispersed in the matrix and randomly oriented in the XY plane, but they were partially ordered in the XZ plane. No signs of fiber degradation were observed and the fibers retained their original shape. As reported in our previous studies [44] the thin organic film deposited on the fiber from the slurry infiltration process acted likely as sacrificial carbon during sintering, therefore minimizing the fiber/matrix interaction.

The mechanical properties of the sample ZS were comparable and in some cases better than samples reinforced with short carbon fibers obtained via ball milling, having the same ceramic matrix and similar carbon fiber content [45]. In fact, the bending strength was similar with around 107 MPa for the ZS sample of the present study and around 103 MPa for the milled fiber reference sample. However, the fracture toughness of the former was significantly higher (3.6 $MPa{\cdot}m^{0.5}$ vs 2.4 $MPa{\cdot}m^{0.5}$). Nonetheless, compared to samples reinforced with continuous carbon fibers, bending strength (107 MPa and 218 MPa, ZS and long fiber, respectively) and fracture toughness (3.6 $MPa{\cdot}m^{0.5}$ and 6.1 $MPa{\cdot}m^{0.5}$, ZS and long fiber, respectively) was significantly lower [46].

3.2. Tribological tests

During the tribological tests, the temperature and coefficient of friction (COF) were measured as a function of the braking time. For every braking test, the COF trend obtained was calculated as an average COF value for that single braking cycle and reported as a data point in the final cumulative test plot. Furthermore, for every braking cycle, the maximum temperature was reported and used as a data point in the final cumulative test plot.

The braking time was the duration of one single braking cycle to a complete stop of the braking disk. Comparing data from the 1st, 5th and 10th cycle in Table 4, little differences for both disk types were observed. Paired with C/C-SiC disk, a maximum difference of 2 s was observed between the first and the last braking cycle so between cold and hot state.

With the steel disk, the braking time showed a slightly larger variation from 1st to 10th cycle and 1 MPa, from 59 to 65 s. Such variation decreased when a pressure of 3 MPa was applied. This could be attributed to a stabilization and a relatively independent behavior to braking conditions with more converted energy per time (power), resulting in a difference of 6 s and 3 s time change for 1 MPa and 3 MPa, respectively.

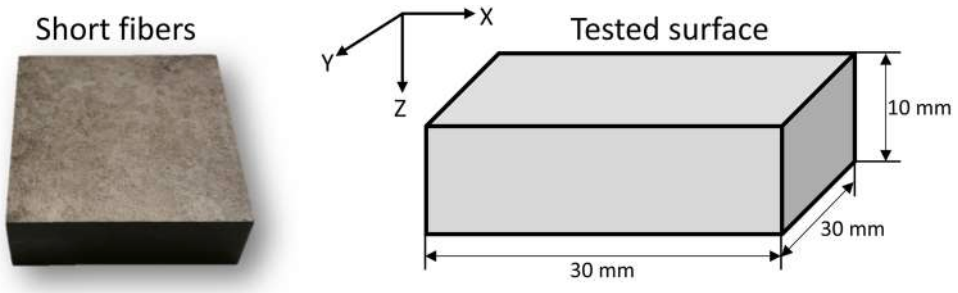

Fig. 2. Macro and schematic images of the sample before testing.

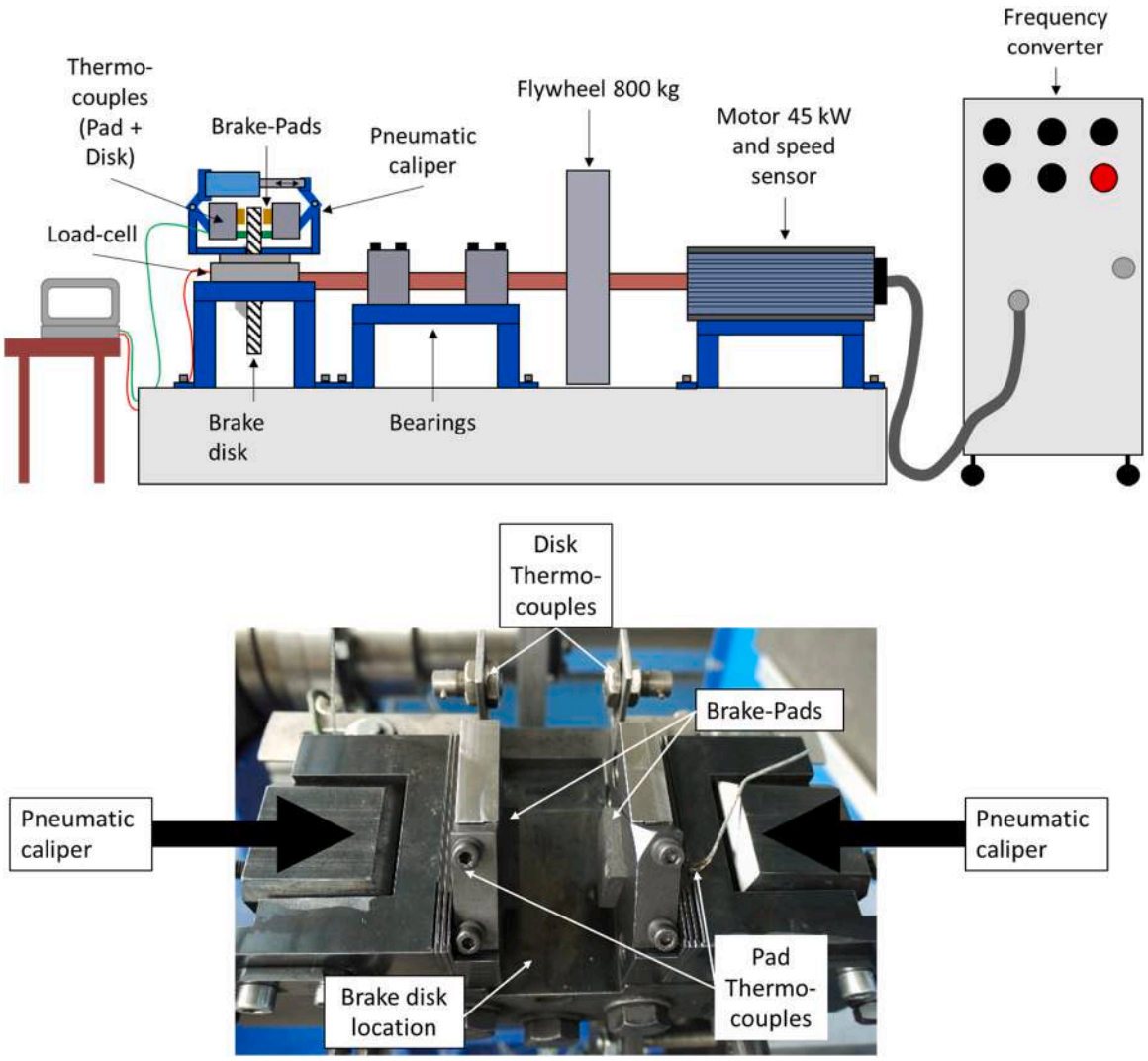

Fig. 3. Top: schematic image of inertia dynamometer; bottom: details of the pads housing and clamps as well as thermocouples.

Table 2
Summary of braking conditions during the tests.

Disk material	Steel	C/C-SiC
cycles per test	10	10
Clamp pressure (MPa)	1 + 3	1 + 3
Sliding speed (m/s)	18.7	20
Friction radius (mm)	173	184
Rotational Speed (rpm)	1030	1030
Energy per 10 cycles (MJ)	≈ 5.4	≈ 5.4

Table 3
Summary of the mechanical properties of the sample [44].

Sample	Density (g/cm^3)	Residual (open) porosity (%)	Bending strength σ (MPa)	K_{IC} ($MPa \cdot m^{0.5}$)	HV 1 (GPa)
ZS	4.1 ± 0.2	6 ± 2	107 ± 13	3.57 ± 0.2	≈ 3.4 ± 0.1

3.2.1. Steel disk

The pads tested (ZS) on a steel disk (Fig. 5) at 1 MPa had an average coefficient of friction of 0.56. The COF was very stable ranging from 0.60 to 0.55 from the first to the last braking test. The single braking test revealed a temperature independent COF behavior, with increasing COF for lower sliding speeds. This increase in COF could be the effect of metal-on-metal adhesion with abraded steel from the disk, as discussed later. The maximum temperature registered was only 365 °C, which was expected due to the low COF and therefore longer period for heat dissipation. The actual temperatures might be higher but measured temperatures were lower due to the distance between pads and thermocouples as well as the not ideal heat transfer to the sliding thermocouples.

During the test at 3 MPa (Fig. 6), the average friction coefficient decreased significantly (0.43) compared to the test at 1 MPa, but it also remained quite stable, with a variation of 0.05 within the braking cycle. The temperature was ~100 K higher due to the higher pressure, but the material behavior was independent from temperature as observed at 1 MPa earlier. In fact, the shapes of single braking curves correspond to the 1 MPa tests and temperatures increased as a result of the decreasing braking times. The little difference in COF and temperature between the test at 1 and 3 MPa show that the material behavior was quite independent of temperature and pressure but sliding speed.

After the tribological tests, the pads and the disks were analyzed by SEM-EDS. Due to the dimensions of the disk, it was not possible to observe their surface in the SEM. For the braking cycles with the steel disk, the disk surface showed evident scratches and grooves after the tribological tests, suggesting material transfer from the disk to the pad (Fig. 7a). On the other hand, the pad wear was negligible (Fig. 7b). The

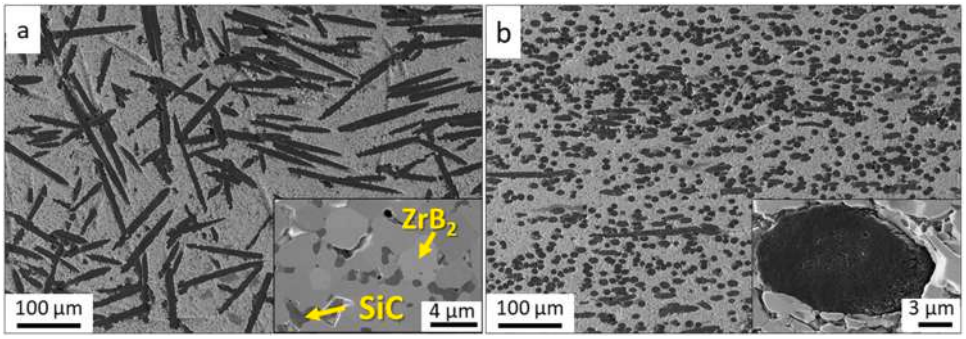

Fig. 4. Surface morphologies before the tests. Light and dark gray phases were ZrB_2 and SiC respectively, while carbon fibers were black: (a) XY plane: random fiber distribution; (b) XZ plane: partial anisotropy imparted by the applied pressure during sintering and detail of the fiber/matrix interface.

Table 4
Analysis of braking time.

Disk Material	Steel Disk		C/C-SiC Disk	
Pressure	1 MPa	3 MPa	1 MPa	3 MPa
Braking 1	59 s	26 s	48 s	-
Braking 5	62 s	27 s	50 s	-
Braking 10	65 s	29 s	50 s	-

material transfer might be caused by the softer nature of the steel disk, which was abraded in the process, therefore avoiding premature failure of the pad. The material removed from the disk probably was transferred to the pad surface and helped the formation of a friction layer that could explain the stable COF observed before (Figs. 5, 6). In contrast, no significant amount of pad material was to the disk surface.

Volumetric and gravimetric wear for the steel disk amounted to 39 mm^3/MJ and 172 mg/MJ for 1 MPa and 55 mm^3/MJ and 246 mg/

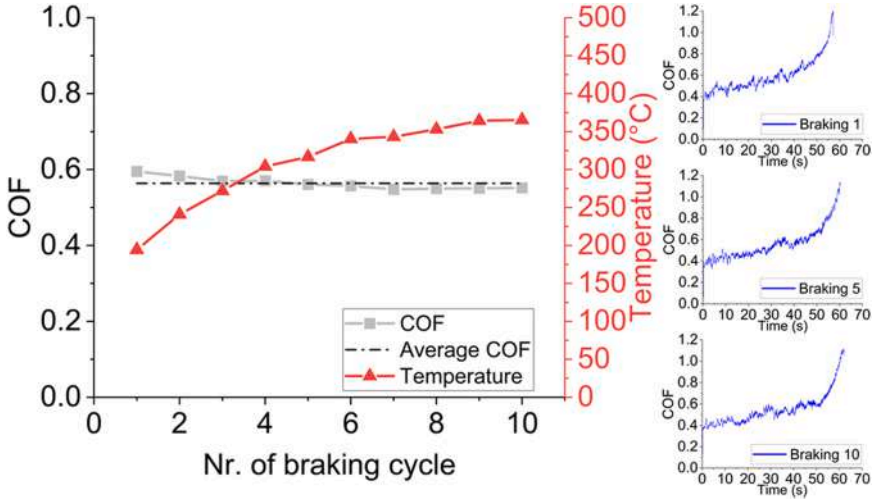

Fig. 5. Average friction coefficient of the ZS material with the steel disk and corresponding disk-temperatures as well as 1st, 5th and 10th braking curve at 1 MPa.

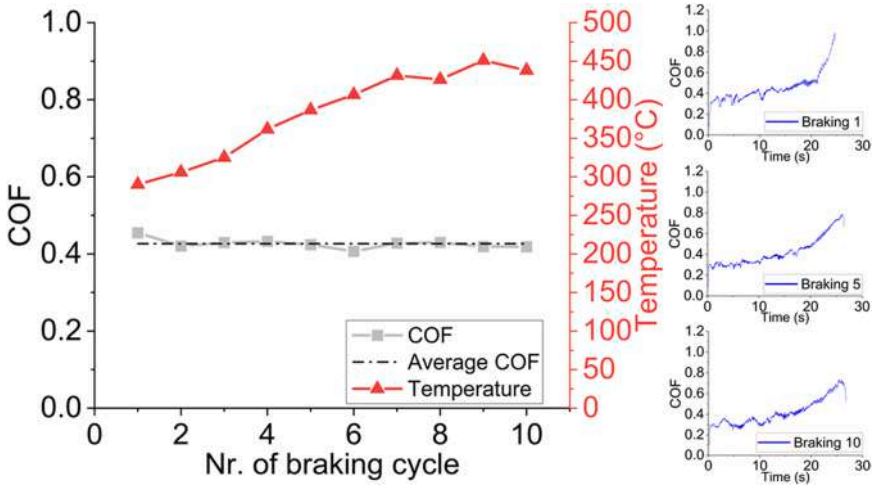

Fig. 6. Average friction coefficient of the ZS material with the steel disk and corresponding disk-temperatures as well as 1st, 5th and 10th braking curve at 3 MPa.

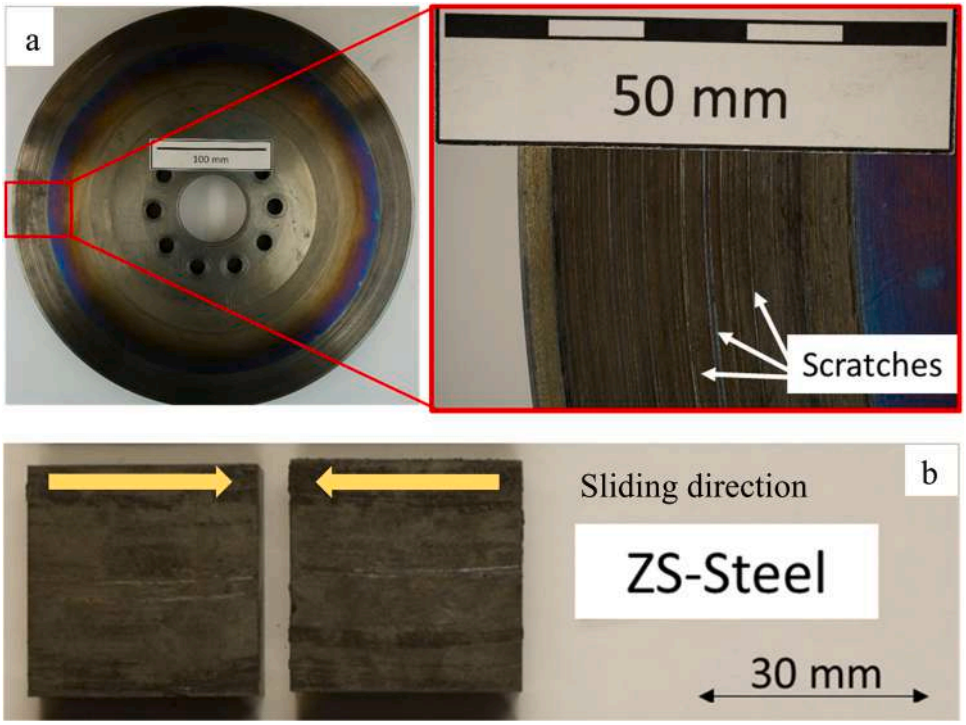

Fig. 7. a) Steel disk after tribological tests at 1 and 3 MPa, showing evident scratches and grooves, b) ZS pads after tribological tests at 1 and 3 MPa, showing no material damage.

MJ for 3 MPa, respectively. Volumetric and gravimetric wear were linear scaled from 1 MPa to 3 MPa, indicating that no material was lost other than on the friction surface. Due to the disk contributing to the formation of friction film, as seen as grooves in the steel disk (Fig. 7a), the relatively low wear rates can be explained.

Also, no signs of mechanical failure of the pads were observed after the braking test. This was due to the soft and ductile nature of the steel disk comparing to the harder surface of the pads. The light blue tempering color on the steel disk indicates that a temperature above 320 °C was reached during the test according to [47].

As for the pad (ZS), microstructural analysis of the surface after wear against the steel disk revealed an uneven friction layer mostly found in spots, with either partially covered (Fig. 8a, b) or fully covered regions (Fig. 8c, d) for both pressures. The partially covered regions still showed

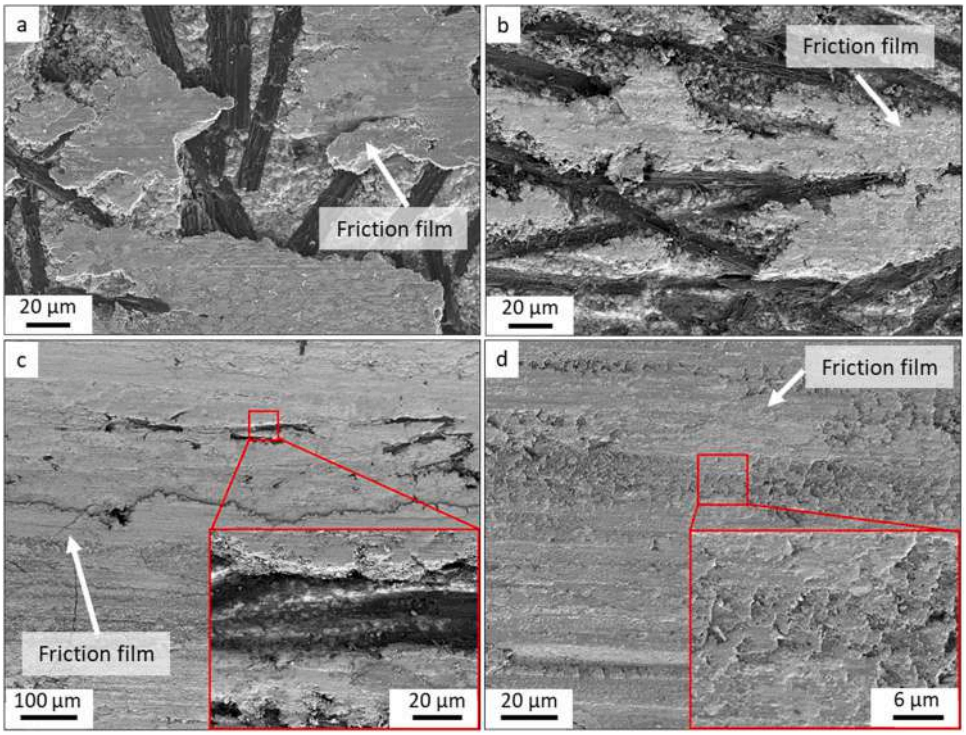

Fig. 8. SEM (SE-mode) images of the sample ZS tested on the steel disk at 1 MPa (a, c) and 3 MPa (b, d). The sliding direction was left to right.

a friction film in direct contact with the disk, as evident by the braking grooves in place of the loose debris. Similarly, a multi-layer structure was present in both pressure conditions. After the test at 3 MPa, the surface was almost entirely covered with a smooth layer of debris (Fig. 8d).

Three different surface compositions were identified (Fig. 9). In some areas the surface maintained the same composition observed before the test, e.g. ZrB_2-SiC-C, as confirmed by EDS analysis (**Spectrum 1**). Other areas were constituted of the same bulk enriched with iron from the disk, with the composition ZrB_2-SiC-C-Fe, (**Spectrum 2**). Finally, inclusions constituted by FeO_x (**Spectrum 3**) were also detected. The iron powder filled the gaps between the ZrB_2-particles, resulting in a flattened surface. The layer was more a film-type version, meaning it had a continuous, smooth, and even surface. The film appeared to be welded out of particles and steel wear dust.

Investigating the cross section (Fig. 10), the friction layer had a thickness ranging from 2 to 10 μm. EDX analysis confirmed the presence of areas with the composition of ZrB_2/ZrO_2-SiC-C-Fe and areas with FeO_x inclusions.

Microstructural analysis suggested that during braking, there was a formation of partially overlapped layers with different compositions. The surface was ground and the detached materials were mixed with the iron from the disk with the formation of a layer constituted by ZrB_2/ZrO_2-SiC-C-Fe. Further grinding led to the formation of a second layer of FeO_x originating from the abraded disk. The friction layer was occasionally shattered in smaller fragments, exposing the underlying material. The fiber orientation is known to significantly affect the braking performance and friction film development [48–50]. Random fiber orientation often proved to be optimal in many braking applications due to a formation of a stable friction film between disk and pads [48]. This stable film can explain the low wear as well as the COF-stability. The resulting amount of steel on the pad surface was able to produce metal on metal adhesion at low sliding speeds. With adhesion forces, a rapidly rising COF is generally expected at the end of a braking cycle as was documented earlier. While this phenomenon causes NVH-issues during stick-slip motion, it can be beneficial for emergency applications, where maximum breaking and holding force is desired.

3.2.2. C/C-SiC disk

The pads tested on the C/C-SiC disk with a force of 1 MPa had an average COF of 0.67 (Fig. 11). Only the first cycle had a slightly higher COF with 0.715, which decreased to 0.67. The registered temperatures were lower as for the steel disk, despite higher COF which might be the result of the ventilated design of the C/C-SiC disk. The temperature increased from 206 °C to 307 °C for the 10th cycle. However, as mentioned before for the tests with the steel disk, the actual disk temperatures might be higher. Single braking cycles showed a very stable COF throughout the entire braking process and only marginal changes in values were observed. A small rise of the COF was observed for low sliding speeds. This rise was far less pronounced than for C/C-SiC or commercial low-met or organic brake pads combined with C/C-SiC disks described by other authors [31,39].

The sample tested at 3 MPa did not survive the test due to strong local mechanical forces inside the pads, which probably exceeded the ZS samples mechanical limits. The C/C-SiC disk after testing did not show evident damage or missing material. Unlike for the steel disk, no grooves or scratches were observed in this case (Fig. 12a). However, a lot of transferred pad material was visible on the surface of the disk in the form of black stains spots. The UHTCMC pad tested against the C/C-SiC disk was characterized by high values of wear, 172 mm^3/MJ for volumetric wear and 692 mg/MJ for gravimetric wear. Due to the C/C-SiC disk not significantly taking part in the wear process, the loss of material in the pads was comparably higher. For classification purpose, this can be compared to C/C-SiC pads on a C/C-SiC-disk from Langhof et al. [38] on the same dynamometer but under varying conditions, where these showed wear rates in between 18 and 130 mm^3/MJ. A full ceramic combination was also proposed by Krenkel et al. [37] where a standard combination of C/C-SiC pairing shows wear rates of about 170 mm^3/MJ with pad and disk combined.

The low volumetric wear of the pads did not match the high mass wear rate if the material density is considered, therefore proving that some material was lost not only on the friction surface but in the whole pad volume. Further evidence of the pads material loss, can be found in the formation of cracks transversal to the friction surface (XY-plane) after the 1 MPa test in Fig. 12b as well as in the XY-plane.

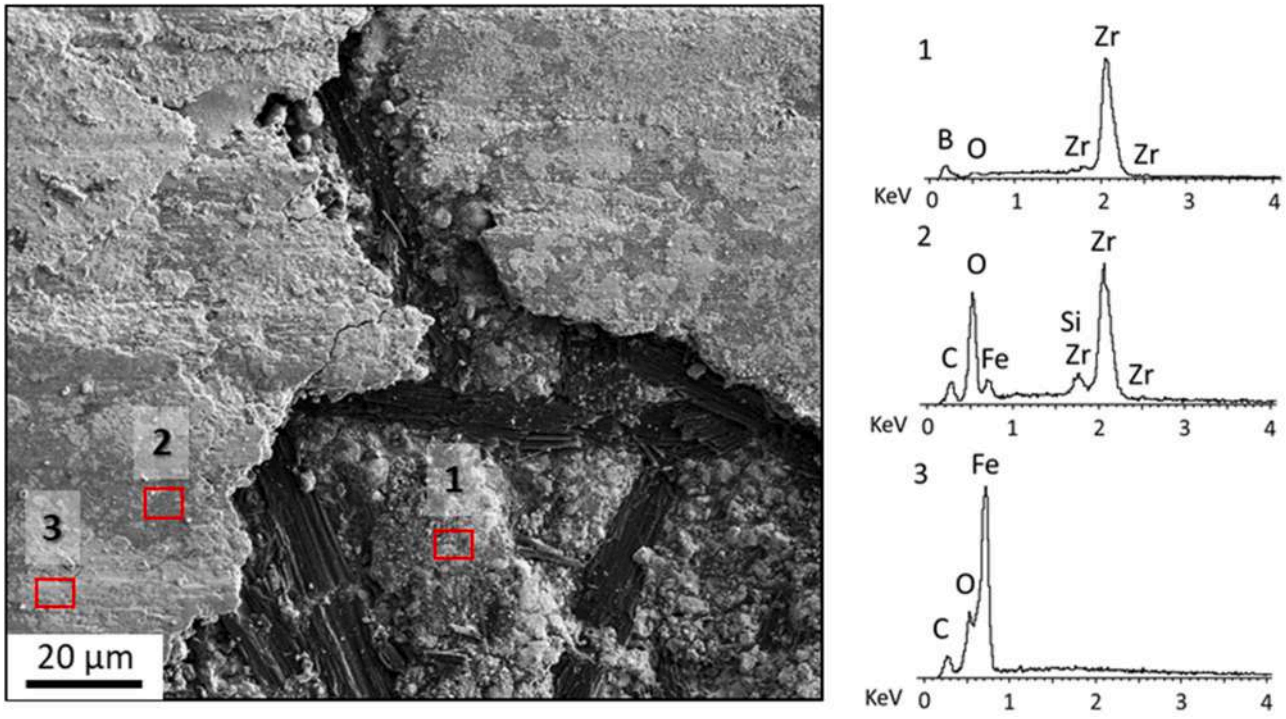

Fig. 9. SEM-images (SE-mode) of a sample tested on a steel disk at 3 MPa with EDX analysis on different spots.

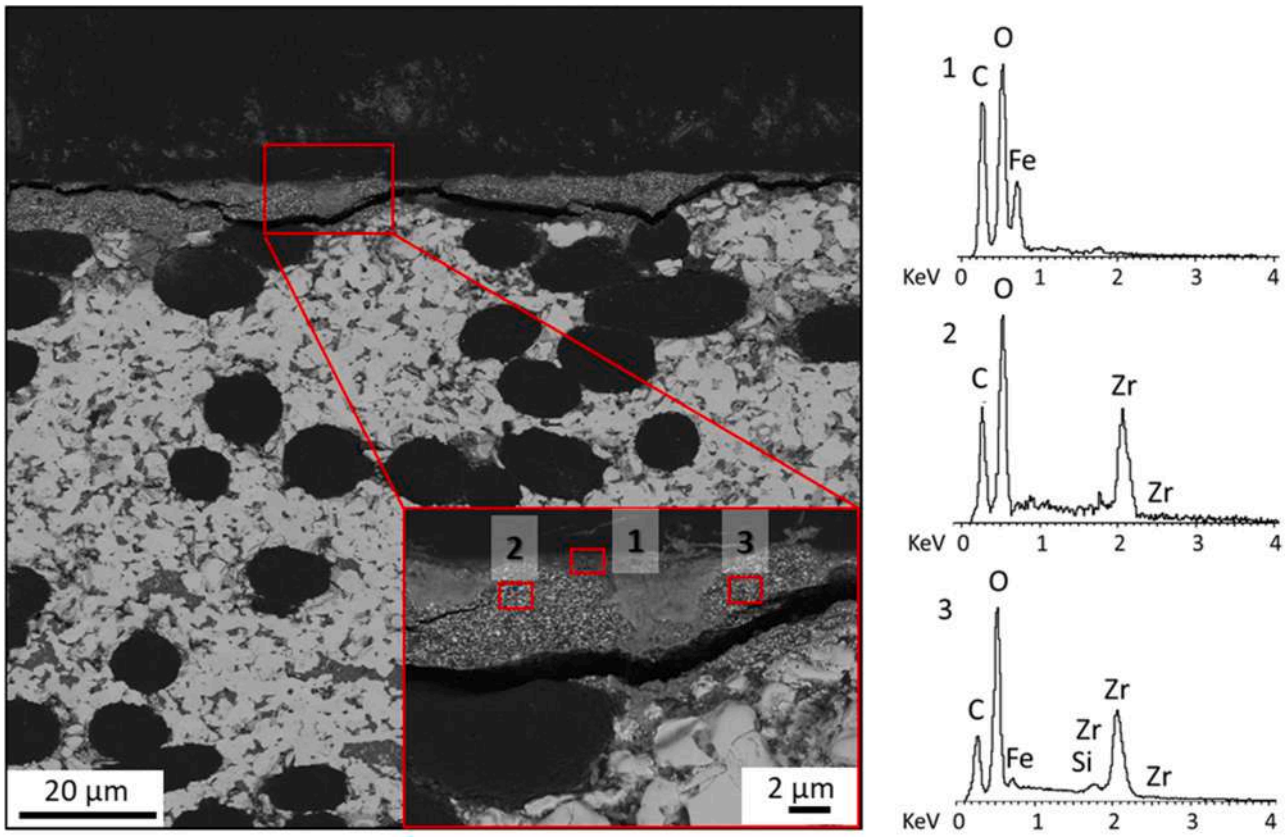

Fig. 10. Section (AsB-mode) of the sample tested on the steel disk at 3 MPa and EDX analysis. (The high amount of C present in the EDX spectrum was due to the carbon coating for SEM analysis and the carbon fiber below the matrix).

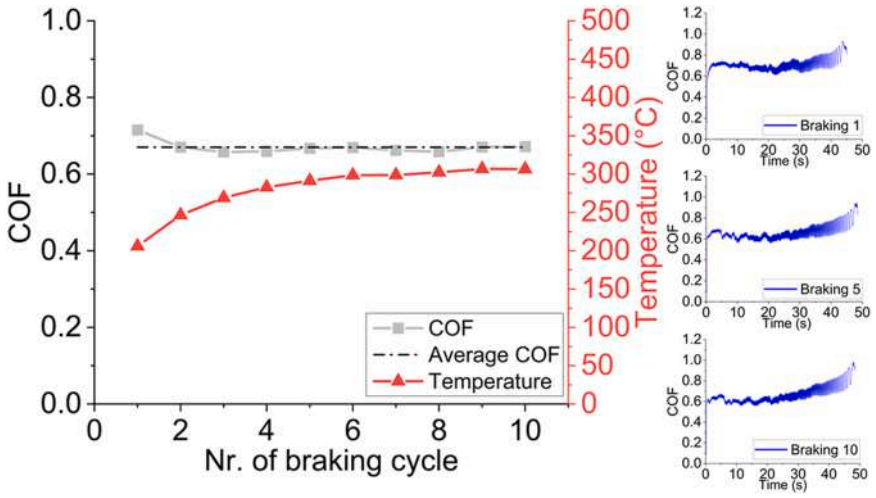

Fig. 11. Average friction coefficient of the ZS material with the C/C-SiC disk and corresponding disk-temperatures as well as 1st, 5th and 10th braking curve at 1 MPa.

From the post-test microstructural analysis of ZS pads surface after testing with the C/C-SiC disk, a friction layer with a texture different from that seen for the steel disk (Fig. 13) was notice. The presence of this stable protective film explains why the mean COF was very stable and independent of the temperature and sliding speed. Moreover, considering the trend of the COF for the single test (Fig. 11) that showed a quite stable behavior, it is believed that a significant friction layer was formed during the first braking cycle. More braking cycles might have improved the thickness of the friction film, but this difference did not seem to affect the braking properties.

The friction film was inhomogeneous on the whole surface, with regions with varying thickness or texture, with a similar layering of the sample tested on the steel disk (Fig. 14). The friction film was thinner and mostly constituted by C/C-SiC or ZrB_2/SiC debris. However, even a small friction layer can stabilize the COF trend.

During the test of the ZS pad, the increase of the pressure from 1 MPa to 3 MPa caused a critical failure of the pads after the first braking cycle (Fig. 15). The cracks generated and their propagation showed a delamination mechanism combined with interlaminar failure in the Z-direction. This issue was likely due to the higher local stresses generated

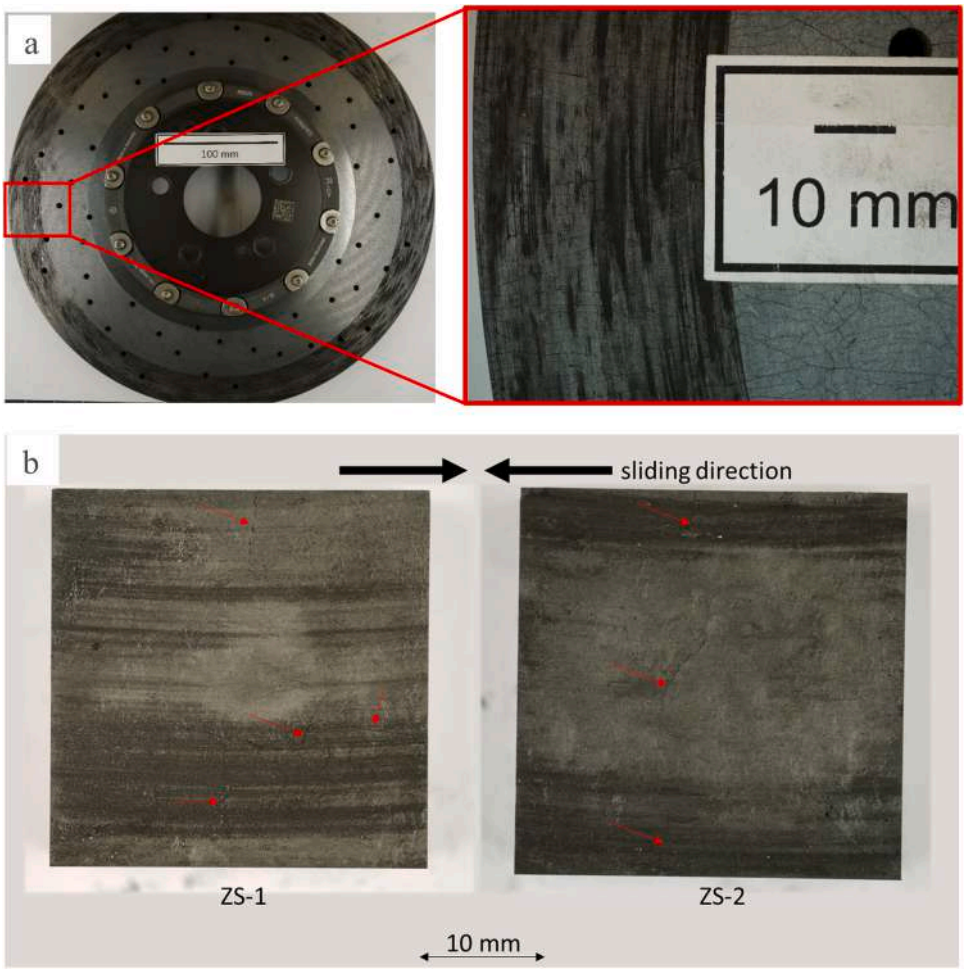

Fig. 12. a) C/C-SiC disk after braking at 1 MPa. A lot of brake pad material was transferred to the disk surface (black). No grooves or missing disk material were observed. b) Sample ZS after testing at 1 MPa, showing the formation of cracks (red arrows).

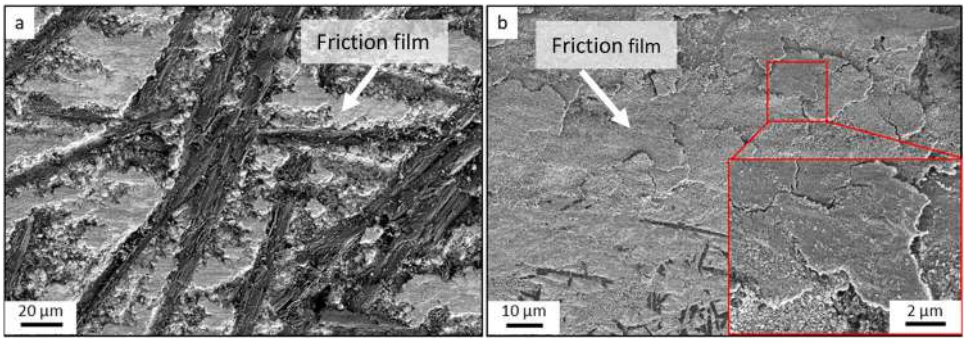

Fig. 13. SEM (SE mode) images of sample ZS tested on C/C-SiC disk at 1 MPa (a, b). The sliding direction is left to right. In the red section a magnification of the friction film is visible.

on the C/C-SiC pads, as evidenced by the high COF already at 1 MPa ($\mu \approx 0.7$), that exceeded the mechanical strength of the pads. The local stresses, coupled with the thin friction layer that did not provide sufficient cushioning between the surfaces and ultimately led to the pad's failure.

3.3. XRD-analysis

X-Ray diffraction was carried out before and after testing the samples with the C/C-SiC and steel disks at 3 MPa in order to identify the species that formed on the surface during braking (Fig. 16). In the XRD pattern, the highest peak was attributed to ZrB_2 (PDF#75–0964), which was the main phase of both samples. Graphite (PDF#75–0444) and SiC-6 H (PDF#19–1131) were detected, in accordance with the EDX analysis. After the braking tests, small amounts of oxides were detected for both specimens: SiO_2 (PDF#47–1144) and ZrO_2 (PDF#50–1089). The EDX analysis identified the presence of Fe on the surface of the sample tested with the steel disk (Fig. 9). The presence of Fe was also confirmed as Fe_2B via XRD.

The presumed reaction is shown below:

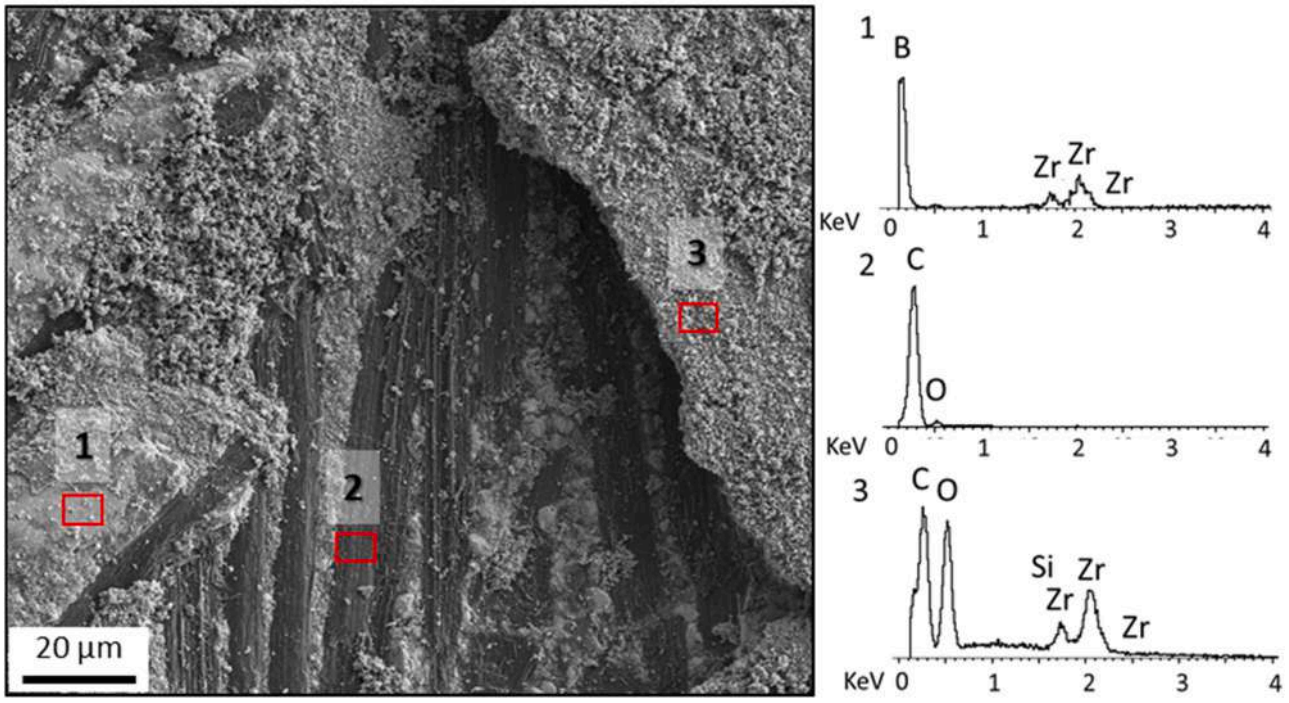

Fig. 14. SEM-images (SE-mode) of a sample tested on a C/C-SiC disk at 1 MPa with EDX analysis on different spots.

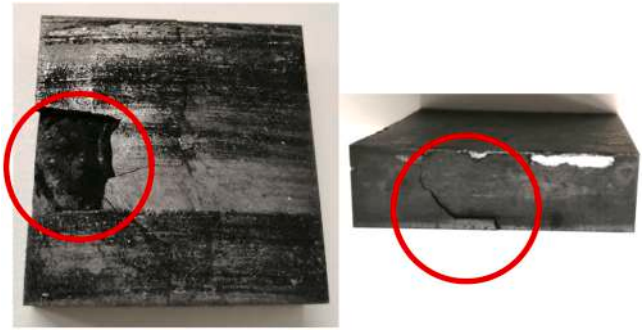

Fig. 15. Sample ZS after testing at 3 MPa on the C/C-SiC disk. Highlighted in red is the material lost and the cracks propagation in the pad.

$$4\ Fe + ZrB_2 + O_2 \rightarrow 2\ Fe_2B + ZrO_2$$

This reaction has a $\Delta G < 0$ in a wide temperature range, from 298 to 1273 K, according to thermodynamic simulations carried out with software Factsage 8.0, but the diffusion of boron atoms in the iron substrate is not kinetically favored below 700 °C [51]. The highest temperature recorded by the thermocouples was around 400–450 °C (Fig. 6), which should not be sufficient for the kinetics of formation of Fe_2B, but the local shear stresses and high pressure suggests that the temperature recorded by thermocouples might have been lower than the real temperature on the sample surface due to the position of the thermocouples located about 60 mm beneath the pads (Fig. 3). Previously studies showed that different position of thermocouples during wear phenomena (e.g. drilling) could cause a variation in temperature observed up to 200 K from the contact point between the surface and the thermocouples position [52].

A direct comparison of the tribological behavior of these composites with other materials studied in previous studies is difficult due to the varying testing conditions and the lack of a unified standard. Many studies on pin on disk type laboratory testers are not applicable to pad on disk studies on inertia dynamometers. Compared to studies of C/C-SiC pads with random fiber orientation (fiber length 12 mm) on steel disks on the same dynamometer at 3 MPa, COF was similar (0.57), but pad wear rate was lower (45 mg/MJ) but also no observation could be made for disk wear [43]. As seen in this study, carbon fiber orientation plays a huge role in COF and especially wear, therefore suggesting the use of a pad material with longer fibers in the future. Previous works on a C/C-SiC disk often report metal on metal adhesion with NVH consequences and a strong "saddle-curved" behavior with low COF at medium speeds [26,34].

ZrB_2-based UHTCMC pads presented a stable COF behavior that is quite independent of temperature or speed due to the formation of a stable friction film with both disk types. For this pad type, mechanical stress was too much at 3 MPa and a hard on hard combination. However, in order to obtain a material with excellent characteristics for braking application, especially at higher loads, pads reinforced with long/continuous carbon fiber will be considered for future studies.

4. Summary and conclusions

Carbon fiber reinforced ZrB_2-10%SiC UHTCMCs were prepared by hot-pressing with randomly orientated chopped carbon fibers. They were tribologically tested on an inertia dynamometer with 1 and 3 MPa against C/C-SiC and steel disks. Afterwards, their microstructure and friction surface were analyzed in detail.

The following conclusions can be drawn:

– In combination with the steel disk, a stable friction film forms, which ensures low wear (≈ 200 mg/MJ) and a stable COF over a large temperature range. The tests showed a mean COF of 0.56 and 0.43 with maximum temperatures of 360 °C and 450 °C for the tests at 1 MPa and 3 MPa, respectively. The multi-layered friction film on the pads consisted out of hard pad particles welded together with abraded steel dust. With this thick friction film, metal on metal adhesion was observed for low sliding speeds. These characteristics of long life, high and quite stable COF were considered appealing for tribological properties.

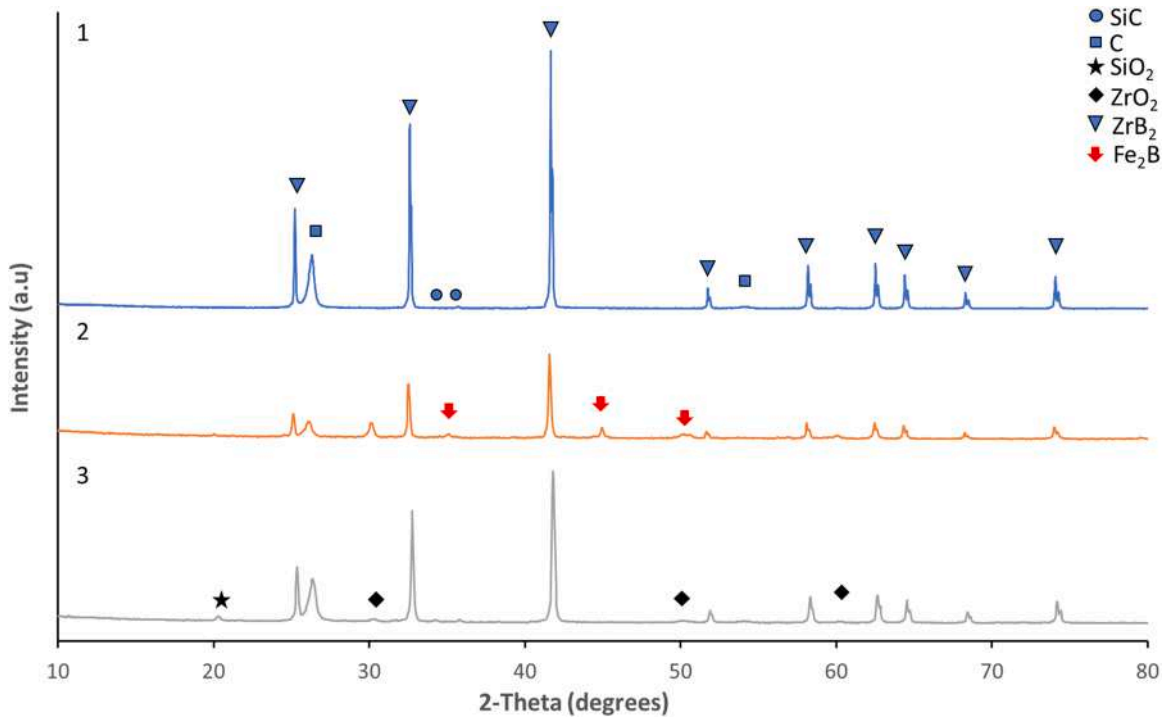

Fig. 16. X-Ray diffraction patterns of UHTCMC-brake pads before (1) and after braking tests at 3 MPa with steel disk (2) and C/C-SiC disk (3). The main peaks are relative to ZrB_2 (PDF#75–0964). Small peaks are relative to SiC-6 H (PDF#19–1131), C (PDF#75–0444), SiO_2 (PDF#47–1144) and ZrO_2 (PDF#50–1089). The presence of Fe_2B was observed on the steel disk (PDF#89–1993).

- The combination with the C/C-SiC disk material shows promising braking behavior at 1 MPa while also inducing mechanical stress on the pads due to the hard on hard combination. The COF was high (0.67), very stable and independent of temperature and showed little saddle-curve-behavior. While wear rate is still high (≈ 500 mg/MJ) because of mechanical material damage attributed to the hard on hard combination, the material combination shows potential for further research.
- The mechanical strength of UHTCMCs must be sufficient to withstand occurring high local forces and vibrations, which vary significantly for comparatively hard and soft counterparts. Short fiber reinforcement is sufficient in combination with softer steel disks or at low pressure in combination with a disk made of C/C-SiC.

The application of ZrB_2 based UHTCMC, reinforced with short carbon fibers as brake material, opened new possibilities for usage of this material class in an application field different from aerospace. In fact, the combination of this material with a steel or C/C-SiC disk showed promising results for braking applications.

Declaration of Competing Interest

The authors declare that they have no known competing financial interests or personal relationships that could have appeared to influence the work reported in this paper.

Acknowledgments

This joint work received funding by the JECS Trust program (contract no. 2020256).

References

[1] M.M. Opeka, I.G. Talmy, E.J. Wuchina, J.A. Zaykoski, S.J. Causey, Mechanical, thermal, and oxidation properties of refractory hafnium and zirconium compounds, J. Eur. Ceram. Soc. 19 (1999) 2405–2414, https://doi.org/10.1016/s0955-2219(99)00129-6.
[2] D.K. Robinson, Temperature Ceramics Temperature Ceramics Materials for Extreme Environment Applications, 2008.
[3] A.L. Chamberlain, W.G. Fahrenholtz, G.E. Hilmas, D.T. Ellerby, High-strength zirconium diboride-based ceramics, J. Am. Ceram. Soc. 87 (2004) 1170–1172, https://doi.org/10.1111/j.1551-2916.2004.01170.x.
[4] S.R. Levine, E.J. Opila, M.C. Halbig, J.D. Kiser, M. Singh, J.A. Salem, Evaluation of ultra-high temperature ceramics for aeropropulsion use, J. Eur. Ceram. Soc. 22 (2002) 2757–2767, https://doi.org/10.1016/S0955-2219(02)00140-1.
[5] A. Vinci, L. Zoli, P. Galizia, D. Sciti, Influence of Y2O3 addition on the mechanical and oxidation behaviour of carbon fibre reinforced ZrB2/SiC composites, J. Eur. Ceram. Soc. 40 (2020) 5067–5075, https://doi.org/10.1016/j.jeurceramsoc.2020.06.043.
[6] L.S. Walker, E.L. Corral, Self-generating high-temperature oxidation-resistant glass-ceramic coatings for C-C composites using UHTCs, J. Am. Ceram. Soc. 97 (2014) 3004–3011, https://doi.org/10.1111/jace.13017.
[7] S. Tang, J. Deng, S. Wang, W. Liu, K. Yang, Ablation behaviors of ultra-high temperature ceramic composites, Mater. Sci. Eng. A 465 (2007) 1–7, https://doi.org/10.1016/j.msea.2007.02.040.
[8] J. Zou, G.J. Zhang, H. Zhang, Z.R. Huang, J. Vleugels, O. Van Der Biest, Improving high temperature properties of hot pressed ZrB 2-20 vol% SiC ceramic using high purity powders, Ceram. Int. 39 (2013) 871–876, https://doi.org/10.1016/j.ceramint.2012.06.018.
[9] J.J. Sha, J. Li, S.H. Wang, Z.F. Zhang, Y.F. Zu, S. Flauder, W. Krenkel, Improved microstructure and fracture properties of short carbon fiber-toughened ZrB2-based UHTC composites via colloidal process, Int. J. Refract. Met. Hard Mater. 60 (2016) 68–74, https://doi.org/10.1016/j.ijrmhm.2016.07.010.
[10] Z. Balak, M. Zakeri, M. Rahimipour, E. Salahi, Taguchi design and hardness optimization of ZrB2-based composites reinforced with chopped carbon fiber and different additives and prepared by SPS, J. Alloy. Compd. 639 (2015) 617–625, https://doi.org/10.1016/j.jallcom.2015.03.131.
[11] F. Yang, X. Zhang, J. Han, S. Du, Characterization of hot-pressed short carbon fiber reinforced ZrB2-SiC ultra-high temperature ceramic composites, J. Alloy. Compd. 472 (2009) 395–399, https://doi.org/10.1016/j.jallcom.2008.04.092.
[12] Z. Nasiri, M. Mashhadi, A. Abdollahi, Effect of short carbon fiber addition on pressureless densification and mechanical properties of ZrB2-SiC-Csf nanocomposite, Int. J. Refract. Met. Hard Mater. 51 (2015) 216–223, https://doi.org/10.1016/j.ijrmhm.2015.04.005.
[13] S. Tang, J. Deng, S. Wang, W. Liu, Comparison of thermal and ablation behaviors of C/SiC composites and C/ZrB2-SiC composites, Corros. Sci. 51 (2009) 54–61, https://doi.org/10.1016/j.corsci.2008.09.037.
[14] D. Sciti, A. Natali Murri, V. Medri, L. Zoli, Continuous C fibre composites with a porous ZrB2 Matrix, Mater. Des. 85 (2015) 127–134, https://doi.org/10.1016/j.matdes.2015.06.136.

[15] A. Vinci, L. Zoli, D. Sciti, J. Watts, G.E. Hilmas, W.G. Fahrenholtz, Influence of fibre content on the strength of carbon fibre reinforced HfC/SiC composites up to 2100 °C, J. Eur. Ceram. Soc. 39 (2019) 3594–3603, https://doi.org/10.1016/j.jeurceramsoc.2019.04.049.
[16] D. Sciti, L. Pienti, A. Natali Murri, E. Landi, V. Medri, L. Zoli, From random chopped to oriented continuous SiC fibers-ZrB2 composites, Mater. Des. 63 (2014) 464–470, https://doi.org/10.1016/j.matdes.2014.06.037.
[17] K. Upadhya, J.M. Yang, W.P. Hoffman, Materials for ultrahigh temperature structural applications, Am. Ceram. Soc. Bull. 76 (1997).
[18] F. Monteverde, A. Bellosi, L. Scatteia, Processing and properties of ultra-high temperature ceramics for space applications, Mater. Sci. Eng. A 485 (2008) 415–421, https://doi.org/10.1016/j.msea.2007.08.054.
[19] P. Hu, Y. Cheng, P. Wang, X. Guo, C. Ma, Q. Qu, X. Zhang, S. Du, Rolling compacted fabrication of carbon fiber reinforced ultra-high temperature ceramics with highly oriented architectures and exceptional mechanical feedback, Ceram. Int. 44 (2018) 14907–14912, https://doi.org/10.1016/j.ceramint.2018.04.249.
[20] J. He, Y. Cao, Z. Li, Y. Wang, Study of tribological properties of polymer derived ZrB2-SiC ceramics, Ceram. Int. 44 (2018) 15627–15630, https://doi.org/10.1016/j.ceramint.2018.05.231.
[21] J.K. Sonber, K. Raju, T.S.R.C. Murthy, K. Sairam, A. Nagaraj, S. Majumdar, V. Kain, Friction and wear properties of zirconium diboride in sliding against WC ball, Int. J. Refract. Met. Hard Mater. 76 (2018) 41–48, https://doi.org/10.1016/j.ijrmhm.2018.05.009.
[22] M. Ivor, D. Medved, M. Vojtko, A. Naughton-Duszova, L. Marciniak, J. Dusza, Nanoindentation and tribology of ZrB2 based luminescent ceramics, J. Eur. Ceram. Soc. 40 (2020) 4901–4908, https://doi.org/10.1016/j.jeurceramsoc.2020.03.021.
[23] M. Mallik, P. Mitra, N. Srivastava, A. Narain, S.G. Dastidar, A. Singh, T.R. Paul, Abrasive wear performance of zirconium diboride based ceramic composite, Int. J. Refract. Met. Hard Mater. 79 (2019) 224–232, https://doi.org/10.1016/j.ijrmhm.2018.12.008.
[24] V. Zamora, C. Ojalvo, F. Guiberteau, O. Borrero-López, A.L. Ortiz, Ultra-low wear B4C-SiC-MoB2 composites fabricated at lower temperature from B4C with MoSi2 additives, J. Eur. Ceram. Soc. 41 (2021) 68–75, https://doi.org/10.1016/j.jeurceramsoc.2021.09.014.
[25] N.L. Savchenko, Yu.A. Mirovoy, A.S. Buyakov, A.G. Burlachenko, M.A. Rudmin, I. N. Sevostyanova, S.P. Buyakova, S.Yu Tarasov, Adaptation and self-healing effect of tribo-oxidizing in high-speed sliding friction on ZrB2-SiC ceramic composite, Wear 446–447 (2020), 203204, https://doi.org/10.1016/j.wear.2020.203204.
[26] N. Savchenko, Y. Mirovoy, A. Burlachenko, I. Sevostyanova, A. Buyakov, M. Rudmin, A. Vorontsov, S. Buyakova, S. Tarasov, Subsurface multilayer evolution of ZrB2–SiC ceramics in high-speed sliding and adhesion transfer conditions, Wear 482–483 (2021), 203956, https://doi.org/10.1016/j.wear.2021.203956.
[27] T.R. Paul, M.K. Mondal, M. Mallik, Abrasive wear performance and wear map of ZrB2-MoSi2-SiCw composites, J. Eur. Ceram. Soc. (2021), https://doi.org/10.1016/j.jeurceramsoc.2021.01.005.
[28] W. Zhang, S. Yamashita, H. Kita, Tribological properties of SiC-B4C ceramics under dry sliding condition, J. Eur. Ceram. Soc. 40 (2020) 2855–2861, https://doi.org/10.1016/j.jeurceramsoc.2020.02.062.
[29] D. Sciti, S. Guicciardi, L. Zoli, S. Failla, C. Melandri, Dry sliding wear behaviour of ZrB2-based ceramics: self-mated and cross coupling with alumina, J. Eur. Ceram. Soc. 42 (2022) 6335–6346, https://doi.org/10.1016/j.jeurceramsoc.2022.07.022.
[30] T. Opel, N. Langhof, W. Krenkel, Development and tribological studies of a novel metal-ceramic hybrid brake disc, Int. J. Appl. Ceram. Technol. 19 (2022) 62–74, https://doi.org/10.1111/ijac.13826.
[31] P. Kumar, V.K. Srivastava, Tribological behaviour of C/C–SiC composites—a review, J. Adv. Ceram. 5 (2016) 1–12, https://doi.org/10.1007/s40145-015-0171-z.
[32] K.H. Breuer, Bert; Bill, Bremsenhandbuch. Grundlagen – Komponenten – Systeme-Fahrdynamik, 2017.
[33] S.K. Rhee, M.G. Jacko, P.H.S. Tsang, The role of friction film in friction wear and noise of automotive brakes, Wear 146 (1991) 89–97, https://doi.org/10.1016/0043-1648(91)90226-k.
[34] Ralph Renz, Entwicklung eines Werkstoff- und Bauweisenkonzepts für keramische Verbundbremsscheiben (Band 14), 2018.
[35] G. Savage, Savage 1993 – Carbon-Carbon Composites.pdf, Chapman & Hall, 1993.
[36] P. Kumar, V.K. Srivastava, A review on wear and friction performance of carbon–carbon composites at high temperature, Int. J. Appl. Ceram. Technol. 13 (2016) 702–710, https://doi.org/10.1111/ijac.12538.
[37] B.H.W. Krenkel, R. Renz, C/C–SiC composites for advanced friction systems, Adv. Eng. Mater. 4 (2002) 427–436, https://doi.org/10.1002/1527-2648(20020717)4:7<427::aid-adem427>3.0.co.
[38] N. Langhof, M. Rabenstein, J. Rosenlöcher, R. Hackenschmidt, W. Krenkel, F. Rieg, Full-ceramic brake systems for high performance friction applications, J. Eur. Ceram. Soc. 36 (2016) 3823–3832, https://doi.org/10.1016/j.jeurceramsoc.2016.04.040.
[39] N. Langhof, R. Voigt, H. Mucha, W. Krenkel, The effect of residual silicon in CMC brake pads on friction and wear, in: Proceedings of the 6th European Conference on Braking JEF 2010, 2010, pp. 1–8.
[40] W. Krenkel, C/C–SiC composites for hot structures and advanced friction systems, in: W.M. Kriven, H.-T. Lin (Eds.), Proceedings of the 27th Annual Cocoa Beach Conference on Advanced Ceramics and Composites B: Ceramic Engineering and Science, Hoboken, John Wiley & Sons, Inc., NJ, USA, 24, 2003, pp. 583–592.
[41] S. Fouquet, M. Rollin, R. Pailler, X. Bourrat, Tribological behaviour of composites made of carbon fibres and ceramic matrix in the Si–C system, Wear 264 (2008) 850–856, https://doi.org/10.1016/j.wear.2006.12.081.
[42] P. Fournier, P. Reynaud, F. Platon, J. Absi, Tribological behaviour of carbon-fibre-reinforced SiC matrix composites, Proc. Inst. Mech. Eng. Part J. J. Eng. Tribol. 214 (2000) 291–306, https://doi.org/10.1243/1350650001543188.
[43] Y. Qian, W. Zhang, M. Ge, X. Wei, Frictional response of a novel C/C-ZrB2-ZrC-SiC composite under simulated braking, J. Adv. Ceram. 2 (2013) 157–161, https://doi.org/10.1007/s40145-013-0055-z.
[44] M. Mor, A. Vinci, S. Failla, P. Galizia, L. Zoli, D. Sciti, A novel approach for manufacturing of layered, ultra-refractory composites using pliable, short fibre-reinforced ceramic sheets, J. Adv. Ceram. 12 (2023) 155–168, https://doi.org/10.26599/JAC.2023.9220674.
[45] D. Sciti, L. Zoli, L. Silvestroni, A. Cecere, G.D. Di Martino, R. Savino, Design, fabrication and high velocity oxy-fuel torch tests of a Cf-ZrB2- fiber nozzle to evaluate its potential in rocket motors, Mater. Des. 109 (2016) 709–717, https://doi.org/10.1016/J.MATDES.2016.07.090.
[46] A. Vinci, L. Zoli, D. Sciti, C. Melandri, S. Guicciardi, Understanding the mechanical properties of novel UHTCMCs through random forest and regression tree analysis, Mater. Des. 145 (2018) 97–107, https://doi.org/10.1016/j.matdes.2018.02.061.
[47] U. Fischer, Tabellenbuch Metall, Haan-Gruiten Verl. Europa-Lehrmittel Nourney, 2001.
[48] W. Zhou, M. Meiser, F. Wich, T. Liensdorf, W. Freudenberg, Y. Li, N. Langhof, W. Krenkel, Fiber orientation dependence of tribological behavior of short carbon fiber reinforced ceramic matrix composites, J. Am. Ceram. Soc. 105 (2022) 538–552, https://doi.org/10.1111/JACE.18075.
[49] E. Fitzer, L.M. Manocha, Carbon reinforcements and carbon/carbon composites, Carbon Reinf. Carbon/Carbon Compos. (1998), https://doi.org/10.1007/978-3-642-58745-0.
[50] T.J. Hutton, D. Johnson, B. McEnaney, Effects of fibre orientation on the tribology of a model carbon-carbon composite, Wear 249 (2001) 647–655, https://doi.org/10.1016/S0043-1648(01)00689-5.
[51] I. Campos-Silva, M. Ortiz-Domínguez, M. Keddam, N. López-Perrusquia, A. Carmona-Vargas, M. Elías-Espinosa, Kinetics of the formation of Fe2B layers in gray cast iron: effects of boron concentration and boride incubation time, Appl. Surf. Sci. 255 (2009) 9290–9295, https://doi.org/10.1016/J.APSUSC.2009.07.029.
[52] M.A. Moghaddas, A.Y. Yi, K.F. Graff, Temperature measurement in the ultrasonic-assisted drilling process, Int. J. Adv. Manuf. Technol. 103 (2019) 187–199, https://doi.org/10.1007/s00170-019-03487-7.